



HAL
open science

Enhanced Photodegradation of Acetaminophen Using Efficient ZnO-NiO Nanofibers

Hassan E Gomaa, Heba H El-Maghrabi, Fatma A Gomaa, Patrice Raynaud,
Amr A Nada

► **To cite this version:**

Hassan E Gomaa, Heba H El-Maghrabi, Fatma A Gomaa, Patrice Raynaud, Amr A Nada. Enhanced Photodegradation of Acetaminophen Using Efficient ZnO-NiO Nanofibers. *Catalysts*, 2024, 14 (7), pp.403. 10.3390/catal14070403 . hal-04744326

HAL Id: hal-04744326

<https://ut3-toulouseinp.hal.science/hal-04744326v1>

Submitted on 18 Oct 2024

HAL is a multi-disciplinary open access archive for the deposit and dissemination of scientific research documents, whether they are published or not. The documents may come from teaching and research institutions in France or abroad, or from public or private research centers.




L'archive ouverte pluridisciplinaire **HAL**, est destinée au dépôt et à la diffusion de documents scientifiques de niveau recherche, publiés ou non, émanant des établissements d'enseignement et de recherche français ou étrangers, des laboratoires publics ou privés.



Distributed under a Creative Commons Attribution 4.0 International License

Article

Enhanced Photodegradation of Acetaminophen Using Efficient ZnO-NiO Nanofibers

Hassan E. Goma^{1,2,3,†} , Heba H. El-Maghrabi^{4,5,†}, Fatma A. Goma^{1,6} , Patrice Raynaud⁴  and Amr A. Nada^{7,8,*}

- ¹ Department of Chemistry, College of Science and Humanities, Shaqra University, Ad-Dawadmi 11911, Saudi Arabia; hjomaah@su.edu.sa (H.E.G.); fjomaah@su.edu.sa (F.A.G.)
² Department of Nuclear Safety Engineering, Nuclear Installations Safety Division, Atomic Energy Authority, Cairo 11765, Egypt
³ Water Research Group, College of Science and Humanities at Ad-Dawadmi, Shaqra University, Ad-Dawadmi 11911, Saudi Arabia
⁴ Laboratoire Plasma et Conversion d'Énergie (LAPLACE), Université de Toulouse, CNRS, INPT, UPS, 31062 Toulouse, France; heba.elmaghrabi@laplace.univ-tlse.fr (H.H.E.-M.); patrice.raynaud@laplace.univ-tlse.fr (P.R.)
⁵ Refining Department, Egyptian Petroleum Research Institute (EPRI), Cairo 11727, Egypt
⁶ Department of Chemistry, College of Women for Science, Arts, and Education, Ain Shams University, Cairo 11757, Egypt
⁷ Department of Analysis and Evaluation, Egyptian Petroleum Research Institute, Cairo 11727, Egypt
⁸ Institut Européen des Membranes, IEM, UMR-5635, Univ Montpellier, ENSCM, CNRS, 34090 Montpellier, France
* Correspondence: amr.nada@umontpellier.fr
† Co-first author.



Citation: Goma, H.E.; El-Maghrabi, H.H.; Goma, F.A.; Raynaud, P.; Nada, A.A. Enhanced Photodegradation of Acetaminophen Using Efficient ZnO-NiO Nanofibers. *Catalysts* **2024**, *14*, 403. <https://doi.org/10.3390/catal14070403>

Academic Editors: Dionissios Mantzavinos, Athanasia Petala and Olga Arvaniti

Received: 17 May 2024
Revised: 20 June 2024
Accepted: 21 June 2024
Published: 26 June 2024



Copyright: © 2024 by the authors. Licensee MDPI, Basel, Switzerland. This article is an open access article distributed under the terms and conditions of the Creative Commons Attribution (CC BY) license (<https://creativecommons.org/licenses/by/4.0/>).

Abstract: The increasing presence of pharmaceutical pollutants, such as acetaminophen, in water bodies poses a significant environmental challenge due to their persistence and potential toxicity. This study investigated the enhanced photodegradation of acetaminophen using ZnO-NiO nanofibers as superior photocatalysts. The nanofibers synthesized with varying NiO contents (designated as ZN0.5, ZN1, ZN1.5, and ZN2), were characterized using X-ray diffraction (XRD), scanning electron microscopy (SEM), Raman, FTIR, Brunauer–Emmett–Teller (BET) analysis, and diffuse reflectance spectroscopy (DRS) to elucidate their structural, morphological, and optical properties. Thermogravimetric analysis (TGA) indicated that the nanofibers exhibit high thermal stability, with major weight loss attributed to the decomposition of the polymer matrix and residual organics. The BET analysis revealed that the specific surface area remains stable after increasing the NiO content up to a certain ratio. This stability correlates with the enhanced photocatalytic performance due to increased light absorption and improved charge separation. The diffuse reflectance spectra and Kubelka–Munk plots demonstrated a reduction in bandgap energy with higher NiO content, facilitating greater visible light absorption. Photocatalytic experiments under visible light irradiation, in the presence of peroxymonosulfate (PMS), showed that the ZN1.5 nanofibers achieved the highest acetaminophen degradation rate, i.e., 92%, within 3 h. Mechanistic studies, supported by radical trapping experiments, revealed that the improved photocatalytic efficiency is due to the synergistic effects of ZnO and NiO heterojunctions, which enhance charge separation and reactive oxygen species (ROS) generation. This research highlights the potential of ZnO-NiO nanofibers as effective photocatalysts for the degradation of pharmaceutical pollutants. The findings demonstrate that optimizing the composition and structure of nanofibers can significantly improve their environmental remediation capabilities, providing a promising solution for sustainable water treatment.

Keywords: environmental remediation; photocatalysis; pharmaceutical contaminants; nanomaterials; zinc oxide; nickel oxide; water treatment

1. Introduction

The presence of pharmaceutical pollutants in aquatic environments has emerged as a pressing environmental concern [1,2]. Among these contaminants, acetaminophen, a widely used analgesic and antipyretic agent, is frequently detected in surface water and groundwater due to its extensive consumption and incomplete removal in conventional wastewater treatment processes [3]. Studies have reported acetaminophen concentrations ranging from 0.01 to 20 µg/L in surface water and up to 6 µg/L in groundwater [4]. In wastewater, concentrations can be significantly higher, ranging from 50 to 1000 µg/L [5,6]. The persistence of acetaminophen in water bodies poses risks to aquatic life and potentially to human health, necessitating the development of effective and sustainable remediation strategies [5].

The removal of pharmaceutical pollutants from fresh water can be addressed through several methods, including processes like flocculation, sedimentation, electrocoagulation, filtration, and chlorination [4,7,8]. While effective for many contaminants, these methods often fall short in fully removing pharmaceutical compounds, which can be highly soluble and resistant to conventional treatments [6]. Advanced treatment technologies such as Adsorption have been explored for the removal of pharmaceutical pollutants. Adsorption methods are effective for removing a wide range of contaminants, including some pharmaceuticals, by adsorbing them onto materials like activated carbon [9–12]. Ozonation and Advanced Oxidation Processes (AOPs) have also been investigated for the degradation of pharmaceutical pollutants. These techniques utilize ozone, hydrogen peroxide, or UV light to break down pollutants into less harmful compounds [13–16]. Membrane technologies, including nano-filtration and reverse osmosis, can physically remove contaminants from water down to the molecular level [17,18].

Photocatalysis has gained significant attention as an advanced oxidation process capable of degrading a wide range of organic pollutants, including pharmaceuticals, into harmless end products [19]. Among the various photocatalytic materials, zinc oxide (ZnO) has garnered considerable attention due to its high oxidative potential, chemical stability, and relatively low cost [20]. ZnO is a wide-bandgap semiconductor that can generate electron–hole pairs upon exposure to ultraviolet (UV) light, leading to the formation of ROS that can degrade organic pollutants. However, the practical application of ZnO is often hindered by its limited absorption in the visible light spectrum and the rapid recombination of photogenerated electron–hole pairs, which reduce its overall photocatalytic efficiency [21].

To address these limitations, researchers have explored the development of hybrid photocatalysts that combine the advantageous properties of different materials. Nickel oxide (NiO), a p-type semiconductor [22], has been identified as an excellent candidate for enhancing the photocatalytic performance of ZnO [23]. The combination of ZnO and NiO in the form of nanofibers can create heterojunctions that facilitate efficient charge separation and broaden the light-absorption range [24].

ZnO-NiO nanofibers offer several advantages over their individual components [25]. The heterojunctions formed between ZnO and NiO can significantly reduce the recombination rate of electron–hole pairs [26], thereby enhancing the generation of ROS and improving the overall photocatalytic activity [27]. Additionally, the high surface area and unique structural properties of nanofibers provide more active sites for photocatalytic reactions, further boosting their efficiency [28].

This study investigated the enhanced photodegradation of acetaminophen, using ZnO-NiO nanofibers as photocatalysts and comparing their performance to that of other commonly used photocatalysts in terms of degradation efficiency and speed. The synthesis, characterization, and photocatalytic performance of these nanofibers are discussed in detail, along with the mechanisms underlying their superior efficiency. The impact of various operational parameters, including the presence of peroxydisulfate (PMS) and visible-light irradiation, on the degradation process is also examined.

By leveraging the synergistic effects of ZnO and NiO, this research aims to provide a deeper understanding of the potential of hybrid nanofiber photocatalysts in addressing

the environmental challenge posed by pharmaceutical pollutants. The findings highlight the importance of optimizing material properties and operational conditions to achieve efficient and sustainable photocatalytic degradation, paving the way for advanced water treatment technologies.

2. Results and Discussion

2.1. Characterization of ZnO-NiO Hybrid Nanofibers

X-ray diffraction (XRD) patterns provide crucial insights into the crystallographic structure of materials. The XRD patterns for ZnO-NiO nanofibers confirm that both NiO and ZnO are present as crystalline phases within the hybrid material (Figure 1). This is evidenced by distinct and identifiable diffraction peaks corresponding to each material: peaks at 37.6° , 43.7° , 63.4° , 75.7° , and 79.8° : These are indexed to the (111), (200), (220), (311), and (222) planes of cubic NiO (PDF #47-1049) crystals in the nanofibers [29].

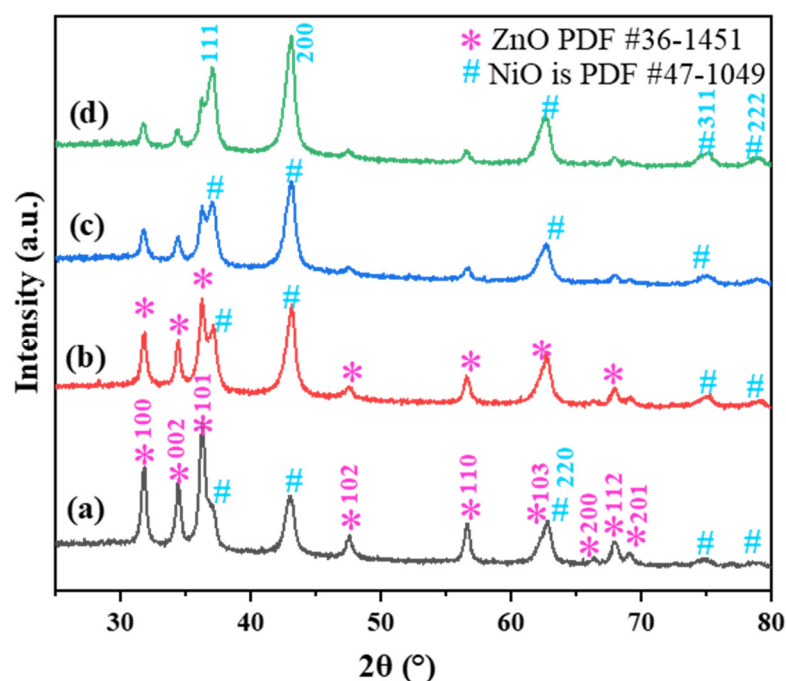


Figure 1. XRD of (a) ZN0.5, (b) ZN1, (c) ZN1.5, and (d) ZN2 nanofibers.

The XRD pattern of ZnO shows that it matches well with the known hexagonal structure of zinc oxide PDF #36-1451, confirming the expected crystal structure. The peaks at 31.7° , 34.4° , 36.2° , 47.5° , 56.6° , 62.9° , 66.4° , 68.0° , and 69.1° are indexed to the (100), (002), (101), (102), (110), (103), (200), (112), and (201) planes of hexagonal ZnO crystals in the nanofibers [30].

The sharpness and intensity of the diffraction peaks are indicative of the high crystallinity of the nanofibers with well-developed and regular lattice structures that are free from significant defects or amorphous areas [31].

High crystallinity is associated with enhanced material properties, such as improved mechanical strength, electrical conductivity, and optical properties, which are crucial for applications as photocatalysts. Thus, the hybrid combination of these materials in a highly crystalline form could leverage the benefits of both, potentially leading to novel functionalities or enhanced performance in hybrid applications [32].

FE-SEM images were used to study the morphology of nanofibers in samples designated as ZN0.5, ZN1, ZN1.5, and ZN2, which varied in regard to the content of NiO (Figure 2). For the ZN0.5 and ZN1 samples, the nanofibers exhibited a rough surface texture. This type of morphology is typically indicative of less uniform growth conditions during synthesis or the presence of multiple nucleation sites, leading to a less ordered crystal structure.

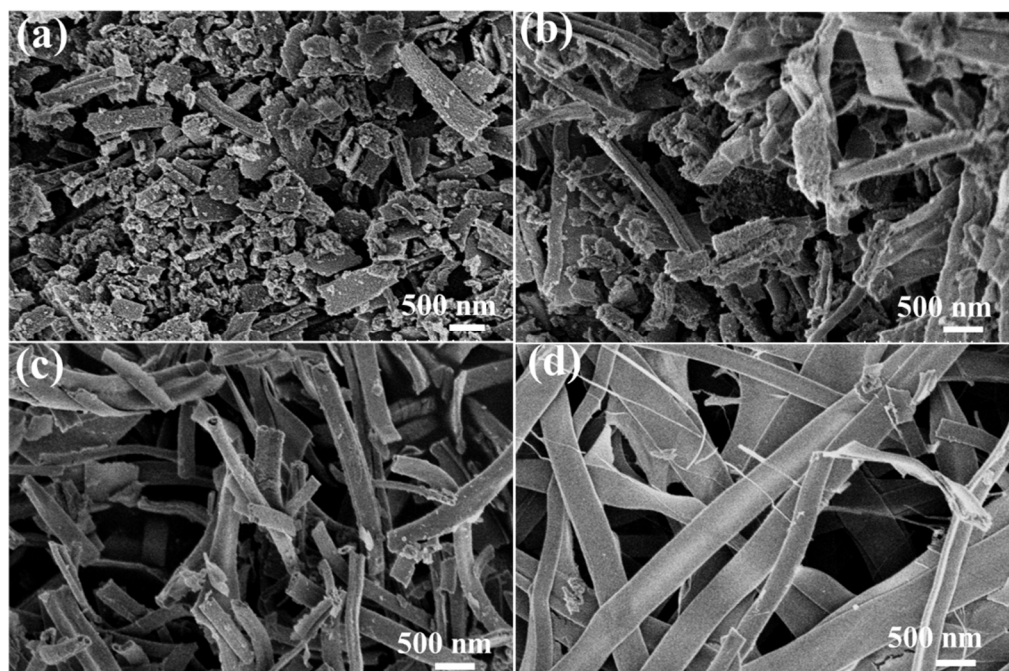


Figure 2. SEM of (a) ZN0.5, (b) ZN1, (c) ZN1.5, and (d) ZN2 nanofibers.

These samples showed nanofibers with relatively short lengths, ranging from 200 to 700 nm. Shorter fibers can result from quicker precipitation or solidification rates during the fiber formation process. As the content of NiO increased in the samples ZN1.5 and ZN2, a noticeable change in the surface morphology was observed. The fibers became smoother and resembled nanowires (NWs), which are typically longer and have more uniform surface characteristics. This transition suggests that NiO might influence the growth kinetics and stabilizing factors in the synthesis process, possibly altering the viscosity or the ionic environment in the reaction medium. The lengths of the nanofibers extended to several micrometers in these samples, which could be a result of prolonged growth phases facilitated by the presence of NiO, leading to more elongated fibers. With an increase in the ratio of nickel, the morphology is affected to a certain degree; as shown in the figure, homogeneous nanofibers can be obtained, which is observed at ZN1.5.

In the FTIR spectra, as illustrated in Figure 3(I), ZnO typically shows a broad absorption band around $400\text{--}600\text{ cm}^{-1}$, which is attributed to the Zn-O stretching vibrations of the ZnO lattice, and the band at 1063 cm^{-1} is attributed to the Zn-O bond. NiO exhibits its characteristic vibrations in the low wavenumber range below 600 cm^{-1} that are associated with Ni-O stretching vibrations.

Given that both ZnO and NiO involve metal–oxygen bonds, their spectral peaks might overlap, particularly in the low wavenumber region. Increasing the NiO content might shift or intensify specific absorption bands, especially around the metal–oxygen stretching region. A higher proportion of NiO could enhance the intensity of the peaks related to Ni-O vibrations. More NiO might also lead to broader bands at certain stretches due to increased disorder or variations in the Ni-O bond environments within the hybrid structure.

Absorption bands around 3400 cm^{-1} (for OH stretching) and 1600 cm^{-1} (for H-O-H bending of water) indicate hydroxyl groups bound to the metal oxides or absorbed water molecules.

By comparing the FTIR spectra of samples with varying NiO contents, we can assess how the incorporation of NiO affects the overall chemical environment and bonding within the hybrid nanofibers. Significant absorption peaks were observed around $1400\text{--}1500\text{ cm}^{-1}$, corresponding to carbonate vibrations, likely from ambient CO_2 capture or residual precursors.

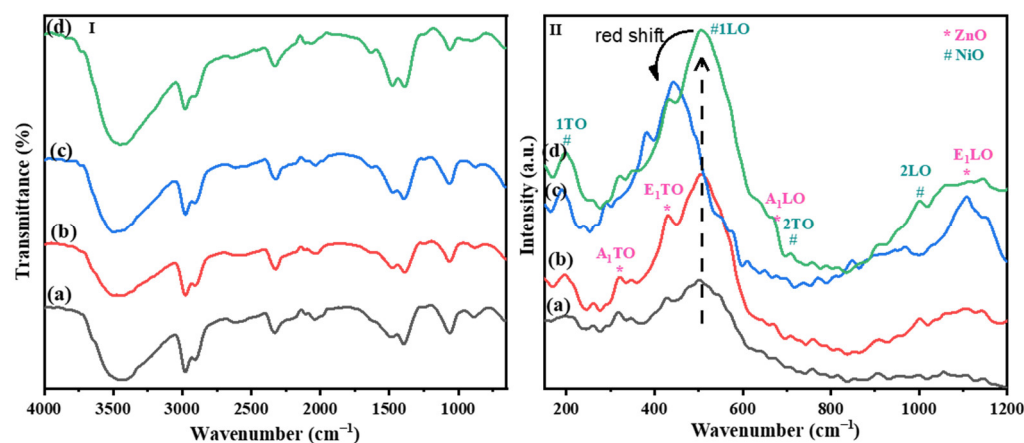


Figure 3. (I) FTIR and (II) Raman of (a) Zn_{0.5}, (b) Zn₁, (c) Zn_{1.5}, and (d) Zn₂ nanofibers.

The Raman spectroscopy of ZnO–NiO hybrid nanofibers provides detailed insights into their structural and vibrational characteristics, which are crucial for understanding the interactions at the molecular level within the hybrid material, as shown in Figure 3(II). The peak at 198 cm^{-1} is typically associated with the first-order transverse optical (TO) phonon mode of NiO. The peak at 506 cm^{-1} corresponds to the longitudinal optical (LO) phonon mode, while the peak at 711 cm^{-1} is assigned to a combination of 2TO phonon modes, indicating a second harmonic generation where two phonons of the same type combine. The peak at 1077 cm^{-1} is attributed to the combination of 2LO phonon modes, another second harmonic process involving longitudinal modes.

For ZnO contributions, the peaks at 320 cm^{-1} and 430 cm^{-1} are associated with the second-order and first-order TO phonon modes, respectively. The presence of these modes in ZnO is typical and signifies standard vibrational characteristics of the crystal lattice involving zinc and oxygen atoms. The peak at 570 cm^{-1} represents a second-order LO phonon mode of ZnO, which overlaps with the LO mode of NiO, indicating a region where the Raman signals of both materials contribute [33]. The peak at 1105 cm^{-1} represents the first-order LO phonon mode of ZnO, indicating higher energy vibrational processes [34].

In the sample Zn_{1.5}, the peak at 506 cm^{-1} is observed to shift by about 65 cm^{-1} compared to its positions in samples with the lowest ratio of NiO. A redshift in Raman spectroscopy generally indicates a reduction in the energy of the phonon modes. This shift can result from substitution or interstitial incorporation, leading to lower frequencies. Additionally, the enhanced electric fields at the interfaces of NiO and ZnO, due to their differing electrical properties, contribute to this redshift. The formation of heterostructures between NiO and ZnO nanocrystals is suggested to lead to the observed redshifts [33].

The evaluation of the porous framework of nanofibers with varying NiO content was conducted using the Brunauer–Emmett–Teller (BET) analysis. This technique provides crucial information about the surface area and porosity of the materials, which are important for their catalytic performance.

The nitrogen adsorption–desorption isotherm for the samples is shown in Figure 4(I). The isotherms exhibit a type-IV shape according to the IUPAC classification, indicating that the nanofibers possess a mesoporous structure. Mesoporous materials have pore sizes between 2 and 50 nm, which are beneficial for catalytic applications due to their high surface area and ability to facilitate mass transport [35]. The presence of a uniform hysteresis loop in the isotherms further confirms the uniformity of the mesoporous structure within the nanofibers. Hysteresis occurs due to capillary condensation within the mesopores [36]. The specific surface area values obtained from the BET analysis for the samples Zn_{0.5}, Zn₁, Zn_{1.5}, and Zn₂ were $79.21 \pm 4.37\text{ m}^2/\text{g}$, $77.72 \pm 0.79\text{ m}^2/\text{g}$, $74.79 \pm 0.58\text{ m}^2/\text{g}$, and $69.36 \pm 0.49\text{ m}^2/\text{g}$, respectively. The decrease in surface area is not significant until the NiO ratio reaches 1.5%. Beyond this specific amount, the surface area drops. Therefore, at this particular ratio of NiO, the surface area remains almost unchanged, which is crucial

for maintaining photocatalytic activity. A larger surface area is advantageous for catalytic applications because it provides more active sites for the adsorption and degradation of pollutants. In the context of photocatalysis, a high surface area enhances the interaction between the catalyst and the pollutant molecules, thereby improving the overall efficiency of the degradation process [37]. The suitable surface-area-to-volume ratio of the nanofibers facilitates the degradation of acetaminophen and other organic pollutants. This is because the increased surface area allows for more active sites where photocatalytic reactions can occur, leading to higher degradation rates. The BET results indicate that the ZnO/NiO nanofibers, especially those with suitable surface areas, like ZN1.5, are well-suited for applications that require efficient photocatalytic degradation of pollutants.

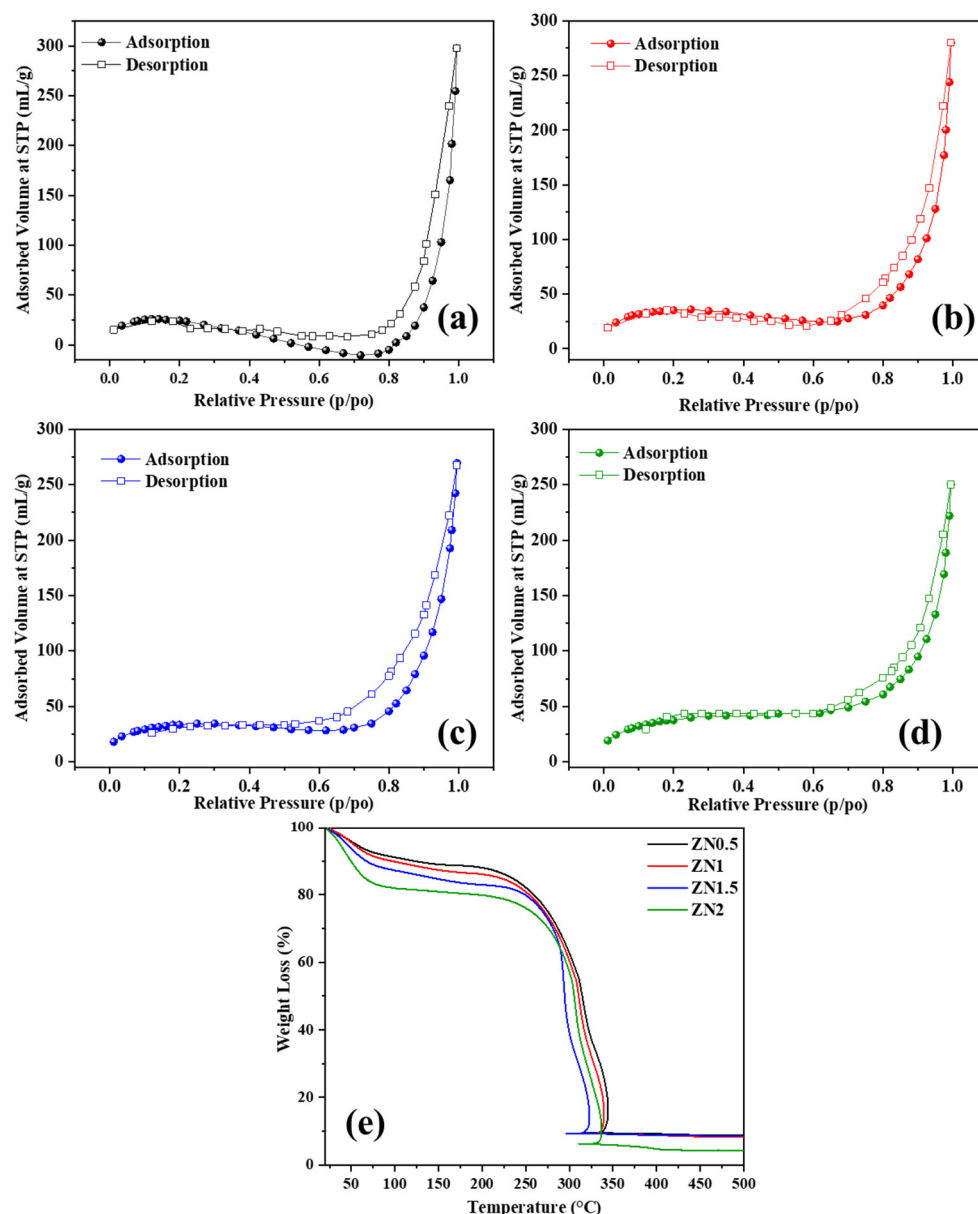


Figure 4. BET of (a) ZN0.5, (b) ZN1, (c) ZN1.5, and (d) ZN2 nanofibers; and (e) TGA of nanofibers.

Thermogravimetric analysis (TGA) curves for ZnO-NiO nanofibers with varying NiO contents are shown in Figure 4(II). The TGA is a technique used to measure the amount and rate of weight change in a material as a function of temperature in a controlled atmosphere.

The TGA curves typically show the weight loss of the samples as the temperature increases. This weight loss is indicative of various processes, such as the removal of adsorbed water, decomposition of organic components, and thermal degradation of the material.

Initial weight loss (up to around 100 °C): This stage is usually associated with the loss of physically adsorbed water and other volatile substances from the surface of the nanofibers. Second stage of weight loss (100 °C to around 300–400 °C): This stage often corresponds to the decomposition of organic residues or any surfactants used during the synthesis of the nanofibers. Final stage of weight loss (above 400 °C): This stage may indicate the thermal degradation or decomposition of the metal oxides and the stabilization of the material. The weight stabilizes after 400 °C, indicating that most decomposable components have been removed and the remaining structure is thermally stable. TGA nanofibers exhibit a similar pattern, but the weight loss is less pronounced with increasing the NiO content, indicating lower amounts of organic residues or a different composition affecting the thermal stability and suggesting a different thermal decomposition behavior due to the higher NiO content. The lower weight loss in samples with higher NiO contents (ZN1.5 and ZN2) suggests that NiO contributes to the thermal robustness of the nanofibers. This makes these materials potentially more stable under operational conditions involving elevated temperatures.

The diffuse reflectance spectra and the Kubelka–Munk plots of ZnO (ZN0) and ZnO–NiO nanofibers with varying NiO contents (ZN0.5, ZN1, ZN1.5, and ZN2) are presented in Figure 5. These figures are essential for understanding the optical properties of the nanofibers, particularly their light-absorption characteristics and bandgap energies, which are critical for photocatalytic applications [38].

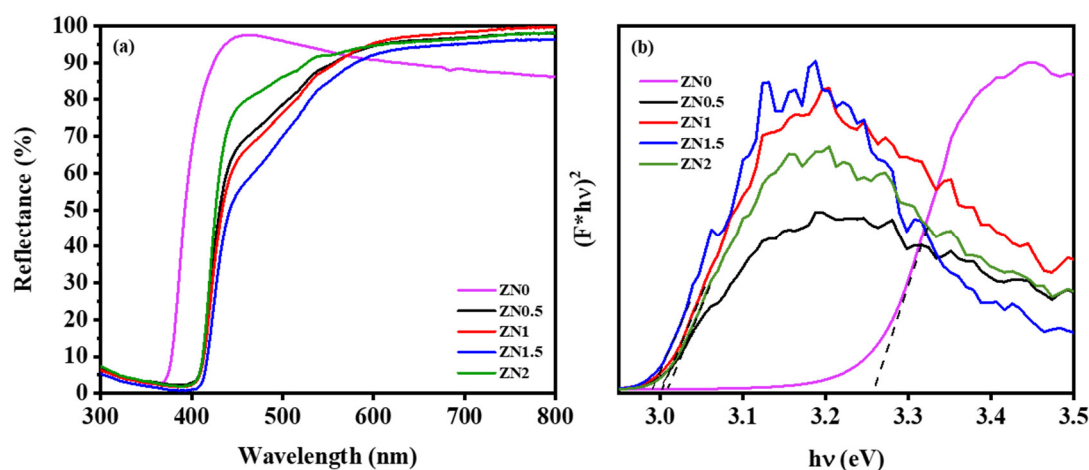


Figure 5. (a) The diffuse reflectance spectra and (b) Kubelka–Munk plots of nanofibers.

The Kubelka–Munk function, $F(R)$, is used to convert reflectance data into a form that can be analyzed to determine the bandgap energy of a material. This function is given by

$$F(R) = (1 - R)^2/2R$$

where R is the reflectance.

The Kubelka–Munk plots are a plot for a direct bandgap, such as $[F(R) \times h\nu]^2$ versus $h\nu$ (where $h\nu$ is the photon energy), to determine the bandgap energy from the intercept of the linear portion of the curve with the x -axis.

The bandgap energy values obtained from the Kubelka–Munk plots for the samples ZN0, ZN0.5, ZN1, ZN1.5, and ZN2 were 3.25, 3.01, 2.99, 2.97, and 3.00 eV, respectively. The value of the bandgap of ZnO nanofibers is consistent with previous studies [39]. The combination of ZnO and NiO in the nanofibers creates a heterojunction that can enhance charge separation and reduce recombination of photogenerated electron–hole pairs, further improving photocatalytic efficiency [40]. The bandgap of the nanofibers decreased with

the increasing Ni content up to a certain ratio (1.5); beyond this point, it increased again due to the agglomeration of NiO on the surface of the nanofibers. The decrease in bandgap with Ni content up to a certain ratio is consistent with previous studies [41]. The variation in optical properties with different NiO contents highlights the importance of optimizing the composition of the nanofibers to achieve the best balance between light absorption and photocatalytic activity.

2.2. Photocatalytic Degradation of Acetaminophen Using ZnO-NiO Hybrid Nanofibers

The photocatalytic degradation of pharmaceutical contaminants like acetaminophen in water is a significant area of research due to the persistence and potential toxicity of these compounds in the environment. In this context, the use of hybrid nanofiber catalysts composed of ZnO and NiO was investigated to enhance the photocatalytic performance under visible-light conditions.

In the experiments, nanofibers with varying contents of NiO (designated as ZN0.5, ZN1, ZN1.5, and ZN2) were tested for their ability to degrade 10 ppm acetaminophen in 210 mL of aqueous solution. The catalysts were used to directly face the incident light. The solution was stirred continuously, and the degradation performance was monitored over a period of 240 min, as illustrated in Figure 6a,b.

The nanofibers demonstrated varying efficiencies, with ZN1.5 showing the highest acetaminophen removal rate at 92%. In contrast, ZN0.5 showed the lowest efficiency at 60%. ZN1 and ZN2 showed intermediate efficiencies of 70% and 80%, respectively. These results suggest that the photocatalytic activity increases with the Ni content up to a certain point, after which it decreases.

Synergistic effects and heterojunctions of ZnO-NiO within the nanofibers are crucial for enhancing photocatalytic efficiency. These heterojunctions facilitate charge transfer and reduce the recombination of electron-hole pairs, which are essential for effective photocatalysis [42]. The presence of NiO at a certain ratio (ZN1.5) correlates with increased photocatalytic activity due to an improved heterostructure, while maintaining the surface area [43].

NiO contributes to shifting the absorption spectrum of the hybrid nanofibers toward the visible range, which significantly enhances acetaminophen degradation under visible light. This shift is critical because it allows the catalyst to utilize a larger portion of the solar spectrum, thereby increasing its practical application potential. In addition, ZnO not only acts as a structural support material, ensuring the durability and stability of the composite during extended photocatalytic processes, but it also functions as a co-catalyst. It enhances the separation of charge carriers, thereby augmenting the overall photocatalytic efficiency through synergistic effects with NiO [44].

A redshift observed in the Raman spectra of the ZN1.5 nanofibers indicates a reduction in the energy of phonon modes, suggesting enhanced charge transport within the material. This shift reduces electronic obstacles, facilitating freer movement of electrons and holes essential for effective photocatalysis.

To test the durability and reusability of the ZN1.5 nanofibers, the same catalyst was used to degrade 10 ppm of acetaminophen in a controlled setup over five consecutive cycles. After each cycle, the catalyst was carefully washed with deionized water to remove any residual chemicals or by-products and then reused under the same experimental conditions.

The degradation efficiency of acetaminophen was monitored for each cycle and documented. Remarkably, the photocatalytic activity of ZN1.5 nanofibers did not show any significant decrease over the five cycles, as depicted in Figure 6c. This consistent performance indicates that the photocatalyst retains its effectiveness, even after multiple uses, which is a critical criterion for practical environmental applications, where cost-effectiveness and operational sustainability are important.

SEM was employed to examine the surface morphology of the ZN1.5 photocatalyst both before and after the five cycles of use. The SEM images (Supplementary Figure S1)

revealed that there were no significant changes in the morphology of the catalyst after repeated use.

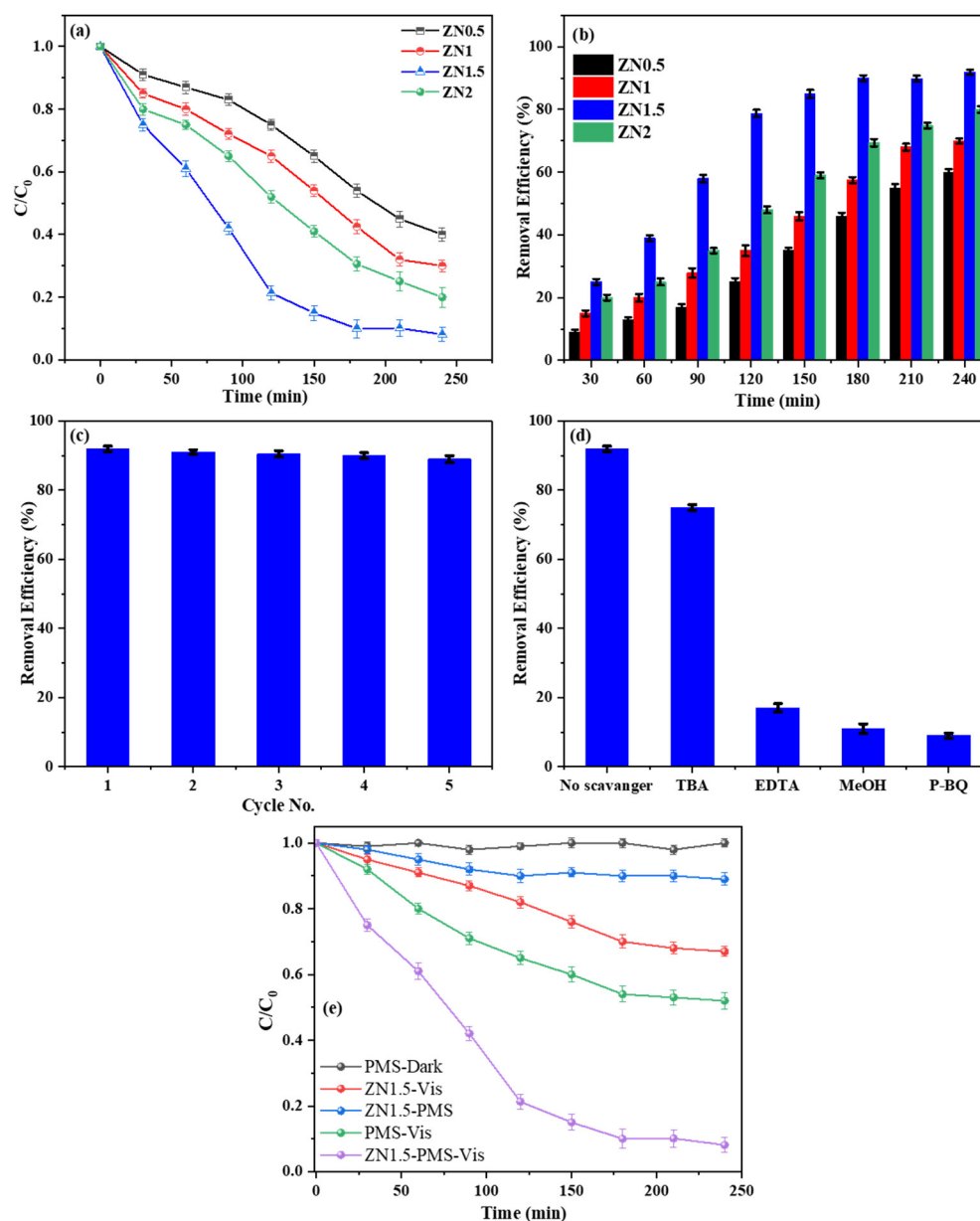


Figure 6. (a) Normalized concentration decay over time for the photocatalytic degradation of 10 ppm acetaminophen under visible light of nanofibers with 0.5 mM PMS. (b) Acetaminophen removal efficiency. (c) Recycling test for ZN1.5 nanofibers. (d) Radical trapping experiments using the indicated scavengers to identify the reactive species involved in acetaminophen degradation with ZN1.5 nanofibers. (e) Comparison of acetaminophen removal under the specified conditions.

The maintenance of the heterostructure morphology is crucial because any degradation or significant morphological changes could impair the photocatalyst's ability to absorb light and generate electron–hole pairs effectively, thus reducing its photocatalytic efficiency.

The findings demonstrate that the ZN1.5 nanofibers are not only effective in degrading pharmaceutical pollutants under visible light but also robust enough to maintain their structural and functional integrity over multiple uses. This durability is advantageous for long-term applications in water treatment facilities, reducing the need for the frequent replacement of catalysts and thus lowering operational costs.

The stability and reusability of the ZN1.5 nanofibers suggest that this material could be scaled up for larger environmental applications. Ensuring that a photocatalyst can withstand repeated use without loss of activity or structural integrity is essential for its implementation in industrial-scale water treatment systems.

The role of reactive species in degradation is illustrated in Figure 6d. Specific scavengers were used to identify the crucial reactive species in the photocatalytic process. The significant drop in degradation efficiency upon the addition of EDTA, methanol (MeOH), and p-benzoquinone (p-BQ) indicates the predominant roles of holes (h^+), sulfate (SO_4^-), and superoxide (O_2^-) radicals, respectively. The addition of tert-butyl alcohol (TBA), which traps hydroxyl radicals (OH), showed a lesser effect, indicating that OH radicals play a minor role in this specific degradation process.

The experiments assessed the effectiveness of ZN1.5 nanofibers under various conditions to activate peroxymonosulfate (PMS) for the degradation of acetaminophen, as presented in Figure 6e. The tests included combinations of ZN1.5 nanofibers, PMS, and visible-light exposure. Conditions such as PMS in the dark alone showed no significant degradation of acetaminophen, underscoring the necessity of a synergistic action between PMS and the photocatalyst under appropriate light conditions to achieve effective degradation [45]. The adsorption in the dark after 240 min using ZN1.5 and PMS was less than 9%, indicating that it is not a significant factor. This intermediate adsorption process served to bring the pollutant to the surface of the catalyst until photodegradation could occur. Moreover, after reusing ZN1.5 over five cycles, no acetaminophen concentration was detected in the washing solution after each cycle, indicating no residual adsorption on the surface of the catalyst. This confirms that the process was primarily due to photodegradation. The ZN1.5 nanofibers combined with PMS under visible light led to significant degradation (92%) of acetaminophen, attributed to the synergistic effects that enhance PMS activation. This is likely due to the generation of reactive sulfate (SO_4^-) radicals facilitated by the photocatalytic action of the nanofibers, which involve the transfer of photogenerated electrons from the ZnO-NiO heterostructure to PMS [46]. Numerous photocatalysts have been developed and assessed for their effectiveness in degrading organic pollutants through photocatalysis. As illustrated in Table 1, the ZnO-NiO nanofiber photocatalyst exhibits a removal performance comparable to other catalysts documented in previous studies. Moreover, it outperforms them in terms of degradation time and efficiency with a lower-power light source.

Table 1. Comparison of photocatalytic efficiency of various composites in organic pollutant degradation.

Pollutant	C (mg/L)	Catalyst	Irradiation Source	Time of Degradation (min)	Removal Efficiency (%)	Ref.
Tetrabromobisphenol A	10	BiVO ₄ /rGO-Cu ₂ O	300 W Xenon lamp	180	91	[47]
Acetaminophen	10	Beta-Bi ₂ O ₃	1000 W Xenon lamp	180	94	[48]
Acetaminophen	1	Cu ₂ O/WO ₃ /TiO ₂	150 W Xenon lamp	60	92	[49]
Acetaminophen	3	g-C ₃ N ₄ -CdS-Bi ₄ O ₅ I ₂ -3	300 W Xenon lamp	25	80	[50]
Acetaminophen	10	CTO-Cu-GO	150 W linear halogen lamp	180	96	[46]
Acetaminophen	5	In ₂ S ₃ /Zn ₂ GeO ₄	Xenon lamp	360	95	[51]
Acetaminophen	10	ZnO-NiO	100 W Xenon lamp	240	92	This work

2.3. Mechanism of ZnO/NiO Heterostructures Nanofibers

The mechanism of the ZnO/NiO heterostructure nanofibers in the context of photocatalytic activity is illustrated in Figure 7. This mechanism explains how the combination of ZnO and NiO in a heterostructure improves the efficiency of photocatalysis by enhancing charge separation and extending light absorption. ZnO is a wide-bandgap semiconductor with a conduction band (CB) and a valence band (VB). The bandgap energy of ZnO is typically around 3.2 eV, which means that it absorbs UV light to generate electron-hole pairs (e^-/h^+).

NiO is a p-type semiconductor. It has a valence band and a conduction band positioned differently from those of ZnO, which helps in the effective separation of charge carriers.

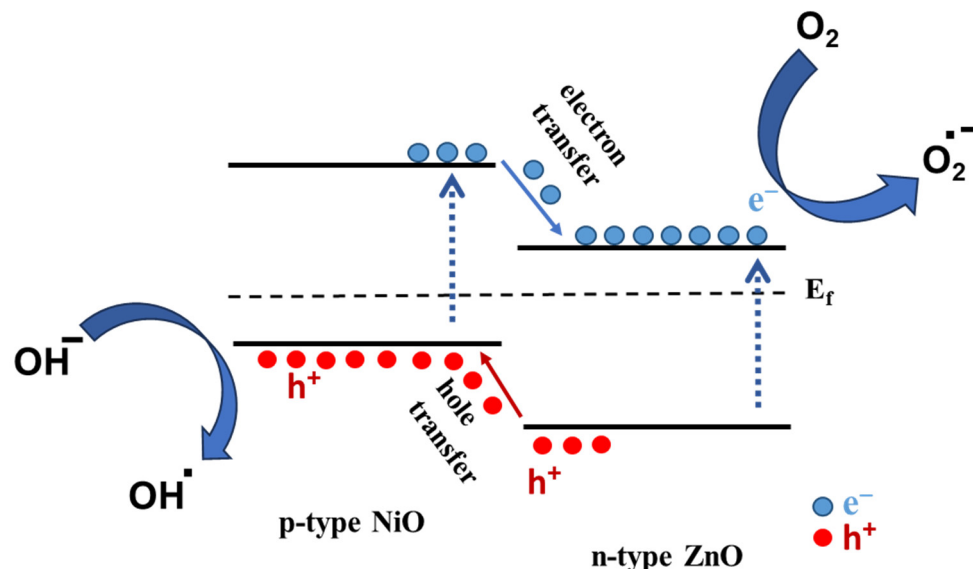


Figure 7. Photocatalytic mechanism of ZnO/NiO heterostructures nanofibers.

When ZnO/NiO heterostructure nanofibers are exposed to visible light, photons with sufficient energy excite electrons (e^-) from the valence band (VB) to the conduction band (CB) in both ZnO and NiO. This leaves behind holes (h^+) in the VB. Due to the heterojunction between ZnO and NiO, the photogenerated electrons and holes are effectively separated. Electrons from the CB of NiO can transfer to the CB of ZnO because the CB of ZnO is at a lower energy level than the CB of NiO. Conversely, holes from the VB of ZnO can migrate to the VB of NiO because the VB of NiO is at a higher energy level than the VB of ZnO. The electrons that accumulate in the CB of ZnO participate in reduction reactions. They can react with oxygen molecules (O_2) in the water to form superoxide radicals ($O_2^{\cdot-}$). The holes in the VB of NiO participate in oxidation reactions. They can oxidize water or hydroxide ions (OH^-) to produce hydroxyl radicals (OH^\bullet).

Formation of Reactive Oxygen Species (ROS): The superoxide radicals ($O_2^{\cdot-}$) and hydroxyl radicals (OH^\bullet) are highly reactive species capable of degrading organic pollutants, such as acetaminophen, into less harmful compounds. These radicals can break down complex molecules into smaller, non-toxic substances. **Enhanced photocatalytic efficiency:** The effective separation of charge carriers (e^- and h^+) reduces their recombination rate, which is a common problem in single-component photocatalysts.

3. Materials and Experimental Methods

3.1. Chemicals and Materials

The following chemicals were acquired and used without further purification: polyvinylpyrrolidone (PVP) with a molecular weight of 1,300,000 g/mol, zinc nitrate hexahydrate (99.99%), nickel nitrate hexahydrate (99.99%), acetic acid (98%), N,N-dimethylformamide (DMF) (99.8%), and acetaminophen (CAS number: 103-90-2) from Sigma Aldrich (St. Louise, MO, USA). Absolute ethanol (99%) was sourced from VWR PROLABO Chemicals, Leicestershire, UK.

3.2. Preparation of ZnO/NiO Nanofibers

Zinc combined with nickel nanofibers was created using the electrospinning technique. The process began by preparing a polymer solution: 1 g of PVP was dissolved in 9 mL of absolute ethanol. To create nanofibers with varying Zn and Ni contents, different molar ratios of Zn:Ni (1:0.05, 1:0.1, 1:0.15, and 1:0.2) were employed. The samples were labeled ZN0.5, ZN1, ZN1.5, and ZN2, with "Z" representing zinc and "N" representing nickel.

Zinc nitrate and nickel nitrate were fully dissolved in 5 mL of N,N-dimethylformamide (DMF), through vigorous stirring, to achieve a homogeneous solution. Then, 0.8 mL of the metal–DMF solution was gradually added to the PVP solution, with gentle stirring, for 2 h. Afterward, 1 mL of acetic acid was introduced to the mixture, which was stirred slowly for an additional hour. The resultant homogeneous solution was extruded through a stainless-steel nozzle with a diameter of 0.7 mm, at a constant flow rate of 0.5 mL/h, regulated by a syringe pump. The electrospinning chamber maintained a temperature of approximately 40 ± 3 °C. Nanofibers were collected on a rotating coil covered with aluminum foil, rotating at 400 rpm. A high voltage of 1.8 KV/cm was applied, with the positive and ground terminals connected to the nozzle and the metallic collector, respectively. During electrospinning, the applied electric field overcame the surface tension of the polymer solution, ejecting a continuous jet. This jet, upon solvent evaporation and bending, formed nanofibers on the collector surface.

3.3. Characterizations of Materials

The crystalline structure of the materials was examined via X-ray diffraction (XRD) using a PANalytical Xpert-PRO diffractometer (Malvern, UK), featuring an Xcelerator detector and Ni-filtered Cu-radiation ($\lambda = 1.54$ Å). Raman spectra were collected using a Horiba XploRA (Palaiseau, France) with a wavelength of 659 nm and a power setting of 20 W. Fourier-transform infrared (FTIR) spectra were obtained with an ATR system on a Nicolet 370 FTIR spectrometer (Thermo Fisher Scientific Inc., Courtaboeuf, France). Scanning electron microscopy (SEM) images were taken with a Hitachi S-4800 (Hitachi High-Tech, Krefeld, Germany). Energy-dispersive X-ray spectroscopy (EDX) and elemental mapping were performed using a Zeiss EVO HD15 microscope paired with an Oxford X-MaxN EDX detector (Zeiss, Paris, France). UV-VIS absorbance spectra were measured using a Jasco V-570 UV-VIS-NIR spectrophotometer (JASCO, Easton, MD, USA). The surface area of the samples was determined by nitrogen adsorption–desorption isotherms at liquid nitrogen temperature, utilizing Micromeritics ASAP 2010 equipment (Micromeritics, Norcross, GA, USA), with outgassing conditions set at 200 °C for 12 h.

3.4. Photocatalytic Reaction

Acetaminophen was utilized as a model pharmaceutical pollutant to test the effectiveness of ZnO/NiO nanofibers in degrading organic compounds. The experiments were conducted in a custom-built Teflon cell containing 210 mL of an aqueous solution with 10 ppm acetaminophen and 0.5 mmol/L PMS. The solution was continuously stirred at 800 rpm. Irradiation was provided by a 100 W xenon lamp. The nanofibers were positioned to face the incident light, with the lamp placed 10 cm from the quartz window. Samples of 1 mL were taken from the solution every 30 min over a total duration of 240 min, using a disposable syringe, and then filtered for analysis.

High-performance liquid chromatography coupled with mass spectrometry (HPLC-MS) was employed to monitor acetaminophen concentration in collected solution aliquots. The HPLC-MS system featured a Waters 2695 pump, an autosampler with a 20 μ L loop, a Waters 2695 separation module, and a Waters Micromass Quattro Micro mass spectrometer equipped with electrospray ionization (ESI). Separation was performed on a Waters XSelect HSS T3 C18 column (100 mm length, 2.1 mm diameter, and 2.5 μ m particle size) at 25 °C. The mobile phase consisted of 97% buffer A (0.1% formic acid in HPLC-grade water) and 3% buffer B (HPLC-grade acetonitrile with 0.1% formic acid) at a constant flow rate of 0.25 mL/min, with a total run time of 3 min.

The triple quadrupole MS operated in positive ESI mode, optimized for maximum sensitivity. Detection settings were as follows: capillary potential of 3.5 kV, cone potential of 25 V, collision energy of 20 V, source temperature of 120 °C, desolvation temperature of 450 °C, cone gas flow rate of 50 L/h, and desolvation gas flow rate of 450 L/h, with nitrogen (99.5% purity) used as the nebulizer gas.

The efficiency of acetaminophen removal was calculated using the following equation:

$$\text{Removal efficiency} = ((C_0 - C)/C_0) \times 100$$

where C_0 (mg/L) is the initial concentration of acetaminophen at time $t = 0$, and C (mg/L) is the concentration at subsequent time points during visible light-induced degradation.

Radical trapping tests with specific scavengers were conducted to identify the primary reactive species involved in acetaminophen degradation. Scavengers included 0.66 mM ethylenediaminetetraacetic acid (EDTA) and 6.6 mM p-benzoquinone (p-BQ) to quench holes (h^+) and superoxide radicals ($\bullet O_2^-$), respectively; and 660 mM tert-butyl alcohol (TBA) and 660 mM methanol (MeOH) to quench hydroxyl radicals ($\bullet OH$) and both sulfate ($\bullet SO_4^-$) and hydroxyl radicals, respectively.

4. Conclusions

This study demonstrates the significant potential of ZnO-NiO nanofibers as effective photocatalysts for the degradation of acetaminophen, a common pharmaceutical pollutant. The ZnO-NiO nanofibers, synthesized with varying NiO content, were extensively characterized to understand their structural, morphological, and optical properties. XRD, SEM, and BET analyses confirmed the successful synthesis of ZnO-NiO nanofibers with mesoporous structures. The BET analysis revealed a decrease in specific surface area with increasing NiO content, highlighting the trade-off between surface area and NiO concentration. TGA analysis indicated high thermal stability of the nanofibers, with major weight loss corresponding to the decomposition of the polymer matrix and residual organics.

Diffuse reflectance spectroscopy and Kubelka–Munk plots showed a reduction in bandgap energy with higher NiO content, enhancing visible-light absorption and photocatalytic activity.

The ZN1.5 nanofibers, containing an optimal NiO content, exhibited the highest acetaminophen degradation rate of 92% within 3 h under visible-light irradiation in the presence of PMS.

The superior photocatalytic performance of ZnO-NiO nanofibers is attributed to the formation of heterojunctions between ZnO and NiO, which enhance charge separation and reduce electron–hole recombination. Radical trapping experiments identified the crucial roles of reactive oxygen species (ROS) such as superoxide radicals (O_2^-) and hydroxyl radicals ($OH\bullet$), generated through the synergistic interaction of the nanofibers and PMS under visible light. The findings underscore the importance of optimizing the composition and structure of nanofibers to achieve enhanced photocatalytic efficiency, paving the way for practical applications in sustainable water treatment.

The study confirms that ZnO-NiO nanofibers can effectively degrade pharmaceutical pollutants, minimizing the formation of toxic intermediates and contributing to safer and cleaner water bodies.

This work provides a solid foundation for the development of advanced photocatalytic materials for environmental remediation and sustainable water treatment technologies.

Supplementary Materials: The following supporting information can be downloaded at <https://www.mdpi.com/article/10.3390/catal14070403/s1>, Figure S1: (a) ZN1.5 before the photocatalytic reaction and (b) Z1.5 after the photocatalytic reaction.

Author Contributions: H.E.G., Formal Analysis, Software, Project Administration, Funding Acquisition, and Writing—Review and Editing; H.H.E.-M., Conceptualization, Methodology, Data Curation, Supervision, Methodology, Validation, Formal Analysis, Investigation, Data Curation, Writing—Original Draft, and Writing—Review and Editing; F.A.G., Methodology, Investigation, Resources, Data Curation, and Writing—Review and Editing; P.R., Methodology, Resources, Supervision, Investigation, and Data Curation; A.A.N., Conceptualization, Methodology, Data Curation, Supervision, Methodology, Validation, Investigation, Data Curation, and Writing—Review and Editing. All authors have read and agreed to the published version of the manuscript.

Funding: The authors extend their appreciation to the Deanship of Scientific Research at Shaqra University for funding this research work through the project number SU-ANN-2023035.

Data Availability Statement: The data supporting the reported results can be made available upon request.

Conflicts of Interest: The authors declare no conflicts of interest.

References

1. Ojha, S.; Tripathi, S.M.; Vishwakarma, P.K.; Mishra, S. Pharmaceuticals in the Water: Emerging Concerns and Innovative Remediation Solutions. *Curr. Green Chem.* **2024**, *11*, 50–62. [[CrossRef](#)]
2. Benny, S.M.; Gupta, S.D.; Ismail, S.P.; Francis, D. Pharmaceutical Pollution of Water Bodies: Sources, Impacts, and Mitigation. In *Handbook of Water Pollution*; John Wiley & Sons, Inc.: Hoboken, NJ, USA, 2024; pp. 371–416.
3. Vo, H.N.P.; Le, G.K.; Nguyen, T.M.H.; Bui, X.-T.; Nguyen, K.H.; Rene, E.R.; Vo, T.D.H.; Cao, N.-D.T.; Mohan, R. Acetaminophen micropollutant: Historical and current occurrences, toxicity, removal strategies and transformation pathways in different environments. *Chemosphere* **2019**, *236*, 124391.
4. Negarestani, M.; Motamedi, M.; Kashtiaray, A.; Khadir, A.; Sillanpää, M. Simultaneous removal of acetaminophen and ibuprofen from underground water by an electrocoagulation unit: Operational parameters and kinetics. *Groundw. Sustain. Dev.* **2020**, *11*, 100474. [[CrossRef](#)]
5. Liu, Z.; Ma, Q.; Dai, L.; Dang, Z. Occurrence, removal and risk evaluation of ibuprofen and acetaminophen in municipal wastewater treatment plants: A critical review. *Sci. Total Environ.* **2023**, *891*, 164600.
6. Lee, W.J.; Goh, P.S.; Lau, W.J.; Ismail, A.F. Removal of pharmaceutical contaminants from aqueous medium: A state-of-the-art review based on paracetamol. *Arab. J. Sci. Eng.* **2020**, *45*, 7109–7135. [[CrossRef](#)]
7. Igwegbe, C.A.; Aniagor, C.O.; Oba, S.N.; Yap, P.-S.; Iwuchukwu, F.U.; Liu, T.; de Souza, E.C.; Ighalo, J.O. Environmental protection by the adsorptive elimination of acetaminophen from water: A comprehensive review. *J. Ind. Eng. Chem.* **2021**, *104*, 117–135. [[CrossRef](#)]
8. Acero, J.L.; Benitez, F.J.; Real, F.J.; Teva, F. Coupling of adsorption, coagulation, and ultrafiltration processes for the removal of emerging contaminants in a secondary effluent. *Chem. Eng. J.* **2012**, *210*, 1–8. [[CrossRef](#)]
9. Rigobello, E.S.; Dantas, A.D.B.; Di Bernardo, L.; Vieira, E.M. Removal of diclofenac by conventional drinking water treatment processes and granular activated carbon filtration. *Chemosphere* **2013**, *92*, 184–191. [[CrossRef](#)] [[PubMed](#)]
10. Skwarczynska-Wojas, A.; Puzskawicz, A. Removal of Acetaminophen from Aqueous Solutions in an Adsorption Process. *Materials* **2024**, *17*, 431. [[CrossRef](#)]
11. Chauhan, A.; Sillu, D.; Agnihotri, S. Removal of pharmaceutical contaminants in wastewater using nanomaterials: A comprehensive review. *Curr. Drug Metab.* **2019**, *20*, 483–505. [[CrossRef](#)]
12. Al-Rub, F.A.A.; Fares, M.M.; Al-Banna, L.N. Toward Cleaner Ecosystems; Elimination of Paracetamol Drug via Mesoporous Activated Carbon Date Pits. *Chem. Sci. Int. J.* **2024**, *33*, 1–21. [[CrossRef](#)]
13. Peralta-Hernández, J.M.; Brillas, E. A critical review over the removal of paracetamol (acetaminophen) from synthetic waters and real wastewaters by direct, hybrid catalytic, and sequential ozonation processes. *Chemosphere* **2023**, *313*, 137411. [[CrossRef](#)] [[PubMed](#)]
14. Roslan, N.N.; Lau, H.L.H.; Suhaimi, N.A.A.; Shahri, N.N.M.; Verinda, S.B.; Nur, M.; Lim, J.-W.; Usman, A. Recent Advances in Advanced Oxidation Processes for Degrading Pharmaceuticals in Wastewater—A Review. *Catalysts* **2024**, *14*, 189. [[CrossRef](#)]
15. Lakshmi, C.N.; Singh, N. Removal of pharmaceutical compounds: Overview of treatment methods. In *New Trends in Emerging Environmental Contaminants*; Springer: Singapore, 2022; pp. 161–180.
16. Inobeme, A.; Ajai, A.I.; Adetunji, C.O.; Munirat, M.; Tsado, M.J.; Mann, A.; Osarenre, J.E.; Inobeme, J.; Mathew, A.; Chinenye, E. Oxidation and advanced oxidation processes in pharmaceutical wastewater treatment. In *Development in Wastewater Treatment Research and Processes*; Elsevier: Amsterdam, The Netherlands, 2024; pp. 157–169.
17. Gupta, S.; Singh, A.; Sharma, T.; Kaur, R.; Khandelwal, V.; Rawat, K.D.; Pathak, S.; Sharma, M.K.; Singh, J.; Shah, M.P.; et al. Applications of ultrafiltration, nanofiltration, and reverse osmosis in pharmaceutical wastewater treatment. In *Development in Wastewater Treatment Research and Processes*; Elsevier: Amsterdam, The Netherlands, 2024; pp. 33–49.
18. Vara, S.; Konni, M.; Karnena, M.K. Membrane technology for treatment of pharmaceutical wastewaters: A novel approach. In *Handbook of Research on Resource Management for Pollution and Waste Treatment*; IGI Global: Hershey, PA, USA, 2020; pp. 502–530.
19. Sanjeev, N.O.; Valsan, A.E. Photocatalytic removal of acetaminophen using green synthesized zinc oxide nanoparticle. In Proceedings of the International Conference on Emerging Trends in Engineering, Hyderabad, India, 28–30 April 2023.
20. Al-Khadhuri, A.; Al-Sabahi, J.; Kyaw, H.H.; Myint, M.T.Z.; Al-Farsi, B.; Al-Abri, M. Photocatalytic degradation toward pharmaceutical pollutants using supported zinc oxide nanorods catalyzed visible light system. *Int. J. Environ. Sci. Technol.* **2023**, *20*, 10021–10030. [[CrossRef](#)]
21. Zyoud, A.H.; Zubi, A.; Hejjawi, S.; Helal, M.H.; Zyoud, S.H.; Qamhieh, N.; Hajamohideen, A.; Hilal, H.S. Removal of acetaminophen from water by simulated solar light photodegradation with ZnO and TiO₂ nanoparticles: Catalytic efficiency assessment for future prospects. *J. Environ. Chem. Eng.* **2020**, *8*, 104038. [[CrossRef](#)]
22. Ahmad, W.; Kaur, N.; Joshi, H.C. Photocatalytic behavior of NiO nanoparticles towards photocatalytic degradation of paracetamol. *Mater. Today Proc.* **2023**, *73*, 36–40. [[CrossRef](#)]

23. Ali, S.M.; Hussein, E.H.; Dakhil, O.A.A. Photocatalytic activity of ZnO/NiO nano-heterojunction synthesized by modified-chemical bath deposition. *Nano Futures* **2021**, *5*, 35001. [[CrossRef](#)]
24. Yousaf, S.; Zulfiqar, S.; Din, M.I.; Agboola, P.O.; Aboud, M.F.A.; Warsi, M.F.; Shakir, I. Solar light irradiated photocatalytic activity of ZnO–NiO/rGO nanocatalyst. *J. Mater. Res. Technol.* **2021**, *12*, 999–1009. [[CrossRef](#)]
25. Dorneanu, P.P.; Airinei, A.; Olaru, N.; Homocianu, M.; Nica, V.; Doroftei, F. Preparation and characterization of NiO, ZnO and NiO–ZnO composite nanofibers by electrospinning method. *Mater. Chem. Phys.* **2014**, *148*, 1029–1035. [[CrossRef](#)]
26. Liu, Y.; Jia, J.; Li, Y.V.; Hao, J.; Pan, K. Novel ZnO/NiO Janus-like nanofibers for effective photocatalytic degradation. *Nanotechnology* **2018**, *29*, 435704. [[CrossRef](#)]
27. Li, J.; Zhao, F.; Zhang, L.; Zhang, M.; Jiang, H.; Li, S.; Li, J. Electrospun hollow ZnO/NiO heterostructures with enhanced photocatalytic activity. *RSC Adv.* **2015**, *5*, 67610–67616. [[CrossRef](#)]
28. Hashim, M.; Usman, M.; Ahmad, S.; Shah, R.; Ali, A.; Rahman, N.U. ZnO/NiO Nanocomposite with Enhanced Photocatalytic H₂ Production. *Int. J. Photoenergy* **2024**, *2024*, 2676368. [[CrossRef](#)]
29. Goel, R.; Jha, R.; Ravikant, C. Investigating the structural, electrochemical, and optical properties of p-type spherical nickel oxide (NiO) nanoparticles. *J. Phys. Chem. Solids* **2020**, *144*, 109488. [[CrossRef](#)]
30. Kavosh, M.; Moallemian, H.; Molaei, H.; Mehranniya, H.; Salami, M.; Dehdashti, M.E. Study of optical and structural properties of zinc oxide nanofibers by using Zn (ac) 2/PVA precursors. *Synth. React. Inorg. Met. Nano-Metal Chem.* **2016**, *46*, 225–229. [[CrossRef](#)]
31. Singh, V.; Sapehia, R.; Dhiman, V. Removal of methylene blue dye by green synthesized NiO/ZnO nanocomposites. *Inorg. Chem. Commun.* **2024**, *162*, 112267. [[CrossRef](#)]
32. Moon, J.; Park, J.-A.; Lee, S.-J.; Lim, S.C.; Zyung, T. Structure and electrical properties of electrospun ZnO–NiO mixed oxide nanofibers. *Curr. Appl. Phys.* **2009**, *9*, S213–S216. [[CrossRef](#)]
33. Qiao, L.; Wang, X.; Sun, X.; Li, X.; Zheng, Y.; He, D. Single electrospun porous NiO–ZnO hybrid nanofibers as anode materials for advanced lithium-ion batteries. *Nanoscale* **2013**, *5*, 3037–3042. [[CrossRef](#)]
34. Truong, T.K.; Nguyen, T.Q.; La, H.P.P.; Le, H.V.; Van Man, T.; Cao, T.M.; Van Pham, V. Insight into the degradation of p-nitrophenol by visible-light-induced activation of peroxymonosulfate over Ag/ZnO heterojunction. *Chemosphere* **2021**, *268*, 129291. [[CrossRef](#)]
35. Bhatia, P.; Nath, M. Green synthesis of p-NiO/n-ZnO nanocomposites: Excellent adsorbent for removal of congo red and efficient catalyst for reduction of 4-nitrophenol present in wastewater. *J. Water Process Eng.* **2020**, *33*, 101017. [[CrossRef](#)]
36. Paul, D.; Maiti, S.; Sethi, D.P.; Neogi, S. Bi-functional NiO-ZnO nanocomposite: Synthesis, characterization, antibacterial and photo assisted degradation study. *Adv. Powder Technol.* **2021**, *32*, 131–143. [[CrossRef](#)]
37. Hallaji, H.; Keshtkar, A.R.; Moosavian, M.A. A novel electrospun PVA/ZnO nanofiber adsorbent for U (VI), Cu (II) and Ni (II) removal from aqueous solution. *J. Taiwan Inst. Chem. Eng.* **2015**, *46*, 109–118. [[CrossRef](#)]
38. Pantò, F.; Dahrouch, Z.; Saha, A.; Patanè, S.; Santangelo, S.; Triolo, C. Photocatalytic degradation of methylene blue dye by porous zinc oxide nanofibers prepared via electrospinning: When defects become merits. *Appl. Surf. Sci.* **2021**, *557*, 149830. [[CrossRef](#)]
39. Xu, Y.; Yan, H.; Chen, T. Application of ZnO/WO₃ Composite Nanofiber Photocatalysts in Textile Wastewater Treatment. *Separations* **2023**, *10*, 339. [[CrossRef](#)]
40. You, J.; Sun, W.; Su, S.; Ao, Z.; Liu, C.; Yao, G.; Lai, B. Degradation of bisphenol A by peroxymonosulfate activated with oxygen vacancy modified nano-NiO-ZnO composite oxides: A typical surface-bound radical system. *Chem. Eng. J.* **2020**, *400*, 125915. [[CrossRef](#)]
41. Zhang, J.; Li, J. The oxygen vacancy defect of ZnO/NiO nanomaterials improves photocatalytic performance and ammonia sensing performance. *Nanomaterials* **2022**, *12*, 433. [[CrossRef](#)] [[PubMed](#)]
42. Puttaraju, T.D.; Soundarya, T.L.; Nagaraju, G.; Lingaraju, K.; Manjula, M.V.; Devaraja, S.; Manjunatha, M. Biogenic approach for synthesis of ZnO/NiO nanocomposites as a highly efficient photocatalyst and evaluation of their biological properties. *Braz. J. Chem. Eng.* **2023**, *1–14*. [[CrossRef](#)]
43. Thampy, U.S.U.; Mahesh, A.; Sibi, K.S.; Jawahar, I.N.; Biju, V. Enhanced photocatalytic activity of ZnO–NiO nanocomposites synthesized through a facile sonochemical route. *SN Appl. Sci.* **2019**, *1*, 1478. [[CrossRef](#)]
44. Sabzehmeidani, M.M.; Karimi, H.; Ghaedi, M. Electrospinning preparation of NiO/ZnO composite nanofibers for photodegradation of binary mixture of rhodamine B and methylene blue in aqueous solution: Central composite optimization. *Appl. Organomet. Chem.* **2018**, *32*, e4335. [[CrossRef](#)]
45. Kohantorabi, M.; Moussavi, G.; Mohammadi, S.; Oulego, P.; Giannakis, S. Photocatalytic activation of peroxymonosulfate (PMS) by novel mesoporous Ag/ZnO@NiFe₂O₄ nanorods, inducing radical-mediated acetaminophen degradation under UVA irradiation. *Chemosphere* **2021**, *277*, 130271. [[CrossRef](#)]
46. Tanos, F.; Makhoul, E.; Nada, A.A.; Bekheet, M.F.; Riedel, W.; Kawrani, S.; Belaid, H.; Petit, E.; Viter, R.; Fedorenko, V.; et al. Graphene oxide-induced CuO reduction in TiO₂/CaTiO₃/Cu₂O/Cu composites for photocatalytic degradation of drugs via peroxymonosulfate activation. *Appl. Surf. Sci.* **2024**, *656*, 159698. [[CrossRef](#)]
47. Chen, K.; Wang, X.; Xia, P.; Xie, J.; Wang, J.; Li, X.; Tang, Y.; Li, L. Efficient removal of 2,2',4,4'-tetrabromodiphenyl ether with a Z-scheme Cu₂O-(rGO-TiO₂) photocatalyst under sunlight irradiation. *Chemosphere* **2020**, *254*, 126806. [[CrossRef](#)] [[PubMed](#)]
48. Xiao, X.; Hu, R.; Liu, C.; Xing, C.; Qian, C.; Zuo, X.; Nan, J.; Wang, L. Facile large-scale synthesis of β-Bi₂O₃ nanospheres as a highly efficient photocatalyst for the degradation of acetaminophen under visible light irradiation. *Appl. Catal. B Environ.* **2013**, *140*, 433–443. [[CrossRef](#)]

49. Chau, J.H.F.; Lai, C.W.; Leo, B.F.; Juan, J.C.; Johan, M.R. Advanced photocatalytic degradation of acetaminophen using $\text{Cu}_2\text{O}/\text{WO}_3/\text{TiO}_2$ ternary composite under solar irradiation. *Catal. Commun.* **2022**, *163*, 106396. [[CrossRef](#)]
50. Li, K.; Chen, J.; Ao, Y.; Wang, P. Preparation of a ternary g- C_3N_4 -CdS/ $\text{Bi}_4\text{O}_5\text{I}_2$ composite photocatalysts with two charge transfer pathways for efficient degradation of acetaminophen under visible light irradiation. *Sep. Purif. Technol.* **2021**, *259*, 118177. [[CrossRef](#)]
51. Yan, T.; Wu, T.; Zhang, Y.; Sun, M.; Wang, X.; Wei, Q.; Du, B. Fabrication of $\text{In}_2\text{S}_3/\text{Zn}_2\text{GeO}_4$ composite photocatalyst for degradation of acetaminophen under visible light. *J. Colloid Interface Sci.* **2017**, *506*, 197–206. [[CrossRef](#)]

Disclaimer/Publisher’s Note: The statements, opinions and data contained in all publications are solely those of the individual author(s) and contributor(s) and not of MDPI and/or the editor(s). MDPI and/or the editor(s) disclaim responsibility for any injury to people or property resulting from any ideas, methods, instructions or products referred to in the content.